

SUPPORTING INFORMATION

Symmetric vs Asymmetric Squaraines as Photosensitizers in Mesoscopic Injection Solar Cells: a Structure-property Relationship Study

Jinhyung Park,^a Claudia Barolo,^{*a} Frederic Sauvage,^{*b} Nadia Barbero,^c Caterina Benzi,^{*d} Pierluigi Quagliotto,^a Salvatore Coluccia,^d Davide Di Censo,^b Michael Graetzel,^b Md. K. Nazeeruddin^b and Guido Viscardi^a

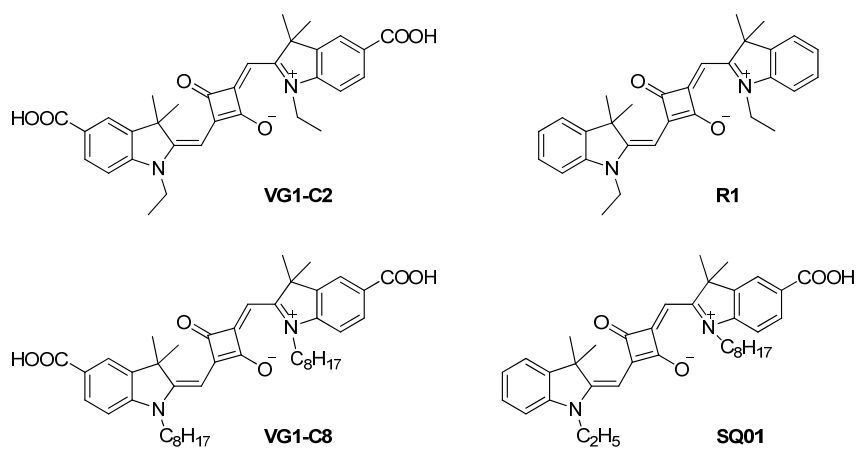
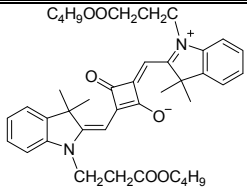
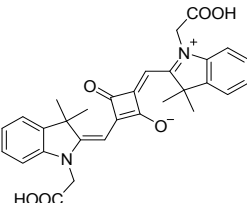
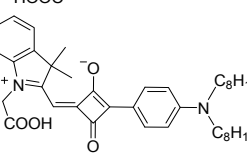
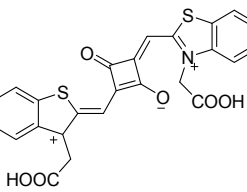
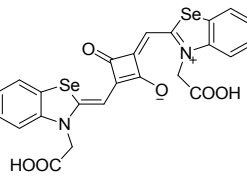
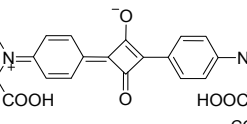
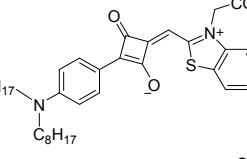
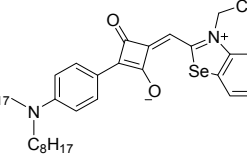
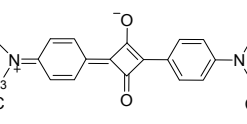
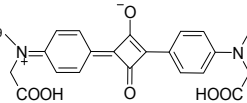
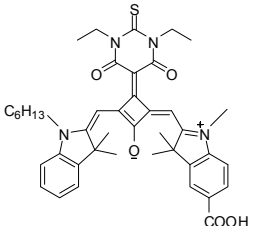
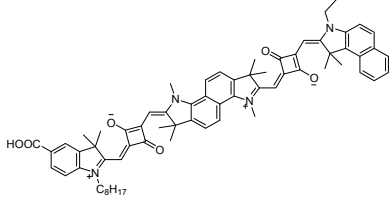
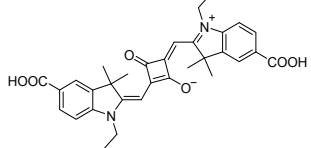
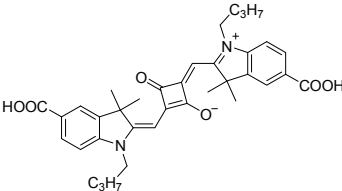
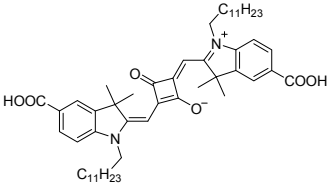
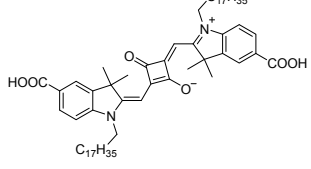
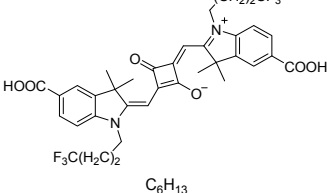
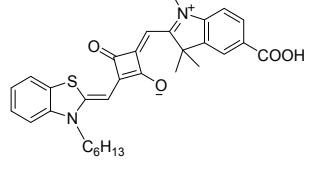
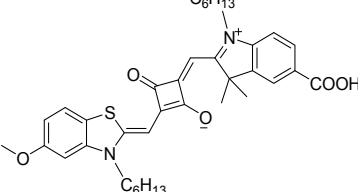


Figure 1-SI Structures of the studied squaraines.

Table 1-SI Detailed literature survey on symmetrical and asymmetrical squaraine DSC sensitizers.

No.	Compound	λ_{abs} [nm]	J_{sc} [mAc m ⁻²]	V_{oc} [V]	FF	η [%]	Ref.
1		631 [ACN]	8.1	0.50	0.59	2.4	[1]
2		637 [ACN]	3.5	0.53	0.53	1.0	[2]
3		620 [ACN]	5.9	0.64	0.53	2.1	[2]
4		- [G]	0.34	0.36	0.46	0.06	[2]
5		- [G]	0.32	0.42	0.52	0.07	[2]
6		628 [ACN]	0.40	0.31	0.53	0.07	[2]
7		600 [ACN]	3.94	0.58	0.53	1.25	[2]
8		611 [ACN]	3.78	0.60	0.61	1.43	[2]
9		-	4.9	0.37	0.53	1.6	[3]
10		-	10.3	0.38	0.52	3.4	[3]

11		642 [MeOH]	11.6	0.49	0.54	3.9	[4]
12		663 [MeOH]	8.6	0.59	0.73	3.7	[5]
13		636 [EtOH]	10.5	0.60	0.71	4.5	[6]
14		662 [DMF]	11.3	0.67	0.72	5.4	[7]
15		632 [MeOH]	2.8	0.45	0.57	1.7	[8]
16		646 [CHCl3]	1.7	0.59	0.28	0.3	[9]
17		662 [THF]	12.8	0.54	0.75	5.2	[10]
18		669 [EtOH]	13.9	0.61	0.74	6.29	[11]

19		642 [ACN]	11.9	0.58	0.68	4.70	[12]
20		730 [DMF]	3.11	0.55	0.76	1.3	[13]
21		640-643 [DMF]	4.03	0.56	0.64	1.46	[14]
22		640-643 [DMF]	4.39	0.58	0.65	1.66	[14]
23		640-643 [DMF]	8.12	0.63	0.69	3.53	[14]
24		640-643 [DMF]	5.40	0.60	0.71	2.29	[14]
25		640-643 [DMF]	6.63	0.57	0.70	2.65	[14]
26		640 [EtOH]	2.0	0.63	0.67	0.85	[15]
27		648 [EtOH]	1.26	0.66	0.66	0.55	[15]

28		691 [EtOH]	11.12	0.42	0.56	2.61	[16]
29		650 [EtOH]	9.40	0.43	0.58	2.34	[16]
30		± 645 [DMF]	7.68	0.60	0.67	3.08	[17]
31		± 643 [DMF]	7.50	0.62	0.72	3.36	[17]
32		659 [EtOH]	14.8	0.64	0.71	6.74	[18]
33		633 [CHCl3]	0.81	0.53	0.65	0.28	[19]
34		632 [CHCl3]	0.39	0.46	0.64	0.11	[19]
35		633 [CHCl3]	1.26	0.55	0.66	0.46	[19]
36		637 [CHCl3]	2.36	0.66	0.71	1.10	[19]

37		-	1.44	0.47	0.63	0.43	[20]
38		-	2.03	0.55	0.68	0.76	[20]
39		-	7.26	0.64	0.68	3.15	[20]
40		-	6.57	0.57	0.65	2.43	[20]
41		650 [THF]	6.6	0.61	0.73	3.0	[21]

- [1] K. Sayama, S. Tsukagoshi, T. Mori, K. Hara, Y. Ohga, A. Shinpou, Y. Abe, S. Suga and H. Arakawa, *Sol. Energy Mater. Sol. Cells*, 2003, **80**, 47-71
- [2] S. Alex, U. Santhosh and S. Das, *Journal of Photochemistry and Photobiology, A. Chemistry*, 2005, **172**, 63-71
- [3] C. Li, W. Wang, X. Wang, B. Zhang and Y. Cao, *Chem. Lett.*, 2005, **34**, 554
- [4] Y. Chen, Z. Zeng, Chao Li, W. Wang, X. Wang and B. Zhang, *New J. Chem.*, 2005, **29**, 773-776
- [5] A. Burke, L. S. Mende, S. Ito and M. Grätzel, *Chem. Commun.*, 2007, **3**, 234-236
- [6] J.-H. Yum, P. Walter, S. Huber, D. Rentsch, T. Geiger, F. Nüesch, F. De Angelis, M. Grätzel, and M. K. Nazeeruddin, *J. Am. Chem. Soc.*, 2007, **129**, 10320-10321
- [7] T. Geiger, S. Kuster, J.-H. Yum, S.-J. Moon, M. K. Nazeeruddin, M. Grätzel and F. Nüesch, *Advanced Functional Materials*, 2009, **19**, 2720-2727
- [8] X. Chen, J. Guo, X. Peng, M. Guo, Y. Xu, L. Shi, C. Liang, L. Wang, Y. Gao, S. Sun and S. Cai, *Journal of Photochemistry and Photobiology, A. Chemistry*, 2005, **171**, 231-236
- [9] F. Silvestri, I. L. Duarte, W. Seitz, L. Beverina, M. V. Martinez-Diaz, T. J. Marks, D. M. Guldi, G. A. Pagani and T. Torres, *Chemical Communications*, 2009, **30**, 4500-4502
- [10] H. Choi, J.-J. Kim, K. Song, J. Ko, M. K. Nazeeruddin and Michael Grätzel, *Journal of Materials Chemistry*, 2010, **20**, 3280-3286
- [11] S. Paek, H. Choi, C. Kim, N. Cho, S. So, K. Song, M. K. Nazeeruddin and J. Ko, *Chemical Communications*, 2011, **47**, 2874-2876.
- [12] L. Beverina, R. Ruffo, C. M. Mari, G. A. Pagani, M. Sassi, F. De Angelis, S. Fantacci, J.-H. Yum, M. Grätzel and M. K. Nazeeruddin, *ChemSusChem*, 2009, **2**, 621-624
- [13] S. Kuster, F. Sauvage, M. K. Nazeeruddin, M. Grätzel, F. A. Nüesch and T. Geiger, *Dyes and Pigments*, 2010, **87**, 30-38

- [14] S. S. Pandey, T. Inoue, N. Fujikawa, Y. Yamaguchi and S. Hayase, *Journal of Photochemistry and Photobiology, A. Chemistry*, 2010, **214**, 269-275
- [15] S. Kim, G. K. Mor, M. Paulose, O. K. Varghese, C. Baik and C. A. Grimes, *Langmuir*, 2010, **26**, 13486-13492
- [16] J.-Y. Li, C.-Y. Chen, C.-P. Lee, S.-C. Chen, T.-H. Lin, H.-H. Tsai, K.-C. Ho and C.-G. Wu, *Organic Letters*, 2010, **12**, 5454-5457
- [17] S. S. Pandey, T. Inoue, N. Fujikawa, Y. Yamaguchi and S. Hayase, *Thin Solid Films*, 2010, **519**, 1066-1071
- [18] Y. Shi, R. B. M. Hill, J.-H. Yum, A. Dualeh, S. Barlow, M. Grätzel, S. R. Marder and M. K. Nazeeruddin, *Angew.Chem.Int.Ed.*, 2011, **50**, 6619-6621
- [19] T. Maeda, H. Nakao, H. Kito, H. Ichinose, S. Yagi and H. Nakazumi, *Dyes and Pigments*, 2011, **90**, 275-283
- [20] T. Inoue, S. S. Pandey, N. Fujikawa, Y. Yamaguchi and S. Hayase, *Journal of Photochemistry and Photobiology, A. Chemistry*, 2010, **213**, 23-29
- [21] J. Warnan, F. Buchet, Y. Pellegrin, E. Blart and F. Odobel, *Organic Letters*, 2011, **13**, 3944-3947

1. Synthesis

All the chemicals were purchased from Sigma Aldrich, and were used as received. The glassware used for the quaternarization syntheses was heated overnight in an oven at 150°C and assembled in the oven, then cooled under Ar flux before starting the reactions. TLC were performed on silica gel 60 F254 plates using DCM and methanol (90:10) as eluents.

ESI-MS spectra (positive ions) were recorded using a LCQ Deca XP plus spectrometer (Thermo), with electrospray interface and ion trap as mass analyzer. The flow injection effluent was delivered into the ion source using nitrogen as sheath and auxiliary gas.

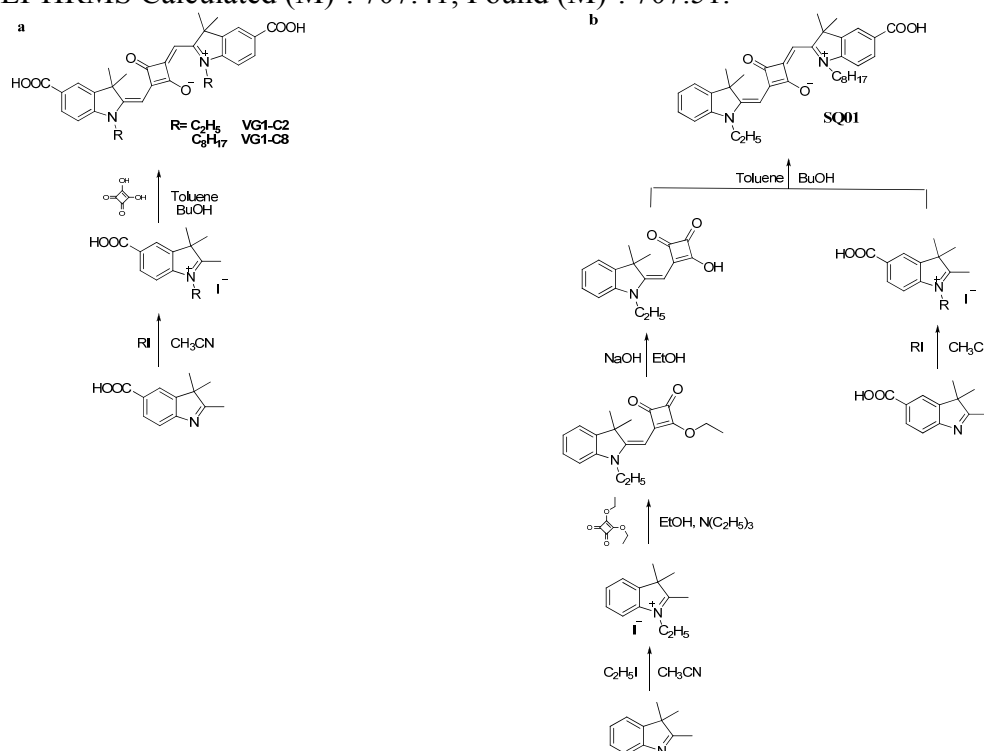
¹H NMR (200 MHz) spectra were recorded on a Bruker Avance 200 NMR in DMSO-d₆ using the DMSO signal as a reference.

All the intermediates, the asymmetrical squaraine **SQ01** and the symmetrical squaraines **R1**, **VG1-C8** and **VG1-C2** were synthesised as reported in literature^{1,2,3}. The symmetrical squaraine **VG1-C8** can be obtained according to a two steps procedure using commercially available precursors (Scheme 1a-SI). This easiness of synthesis comes in opposition to the asymmetrical **SQ01** dye which requires four to five steps combined to two chromatographic purification procedures (Scheme 1b-SI). The purification of VG1-C8 and VG1-C2 was carried out by one or two crystallizations in butanol, affording higher yields with respect to the ones obtained by chromatographic purification.

NMR and ESI-MS analyses are in agreement with the data reported in literature.

SQ01: EI-HRMS Calculated (M)⁻: 579.33; Found (M)⁻: 579.31.

VG1-C8: EI-HRMS Calculated (M)⁻: 707.41; Found (M)⁻: 707.51.



Scheme 1-SI: Comparison between the synthetic pathway of the symmetrical squaraines VG1 (scheme a) and the asymmetrical SQ01 (scheme b).

¹ J-H. Yum, P. Walter, S. Huber, D. Rentsch, T. Geiger, F. Nüesch, F. De Angelis, M. Grätzel, M. K. Nazeeruddin *J. Am. Chem. Soc.*, 2007, 129, 10320–10321

² S. S. Pandeya, T. Inouea, N. Fujikawaa, Y. Yamaguchib, S. Hayase, *J. Photochem. Photobiol A: Chemistry*, 2010, 214, 269-275

³ N. Kuramoto, K. Natsukawa, K. Asao *Dyes and Pigments*, 1989, 11, 21-35.

2. Experimental procedures

2.1 UV spectra - Determination of the λ_{\max} and molar absorption coefficients

Every dye was weighed, (7-10 mg), and diluted to 10 ml in a flask using DMSO. From this solution, 0.25 ml were taken and diluted to 25 ml with the proper solvent (mother solution). Three dilutions were prepared by diluting 1.0, 2.5 and 5 ml of this solution to 25 ml. Those solutions were analyzed by UV-Vis spectroscopy (Cary 300 Bio) using quartz cuvettes (1 cm pathway length). Absorbance at the λ_{\max} for every daughter solution was plotted vs. dye concentration and a linear fitting was performed. The slope of the plot is the molar absorption coefficient (ϵ). The determination was made, in duplicate, by preparing two separate concentrated dye mother solutions in DMSO which were subjected to the same dilution procedure. The $\log \epsilon$ obtained from the two separate data set were compared: if their difference is less or equal to 0.02 respect to their average, the data were considered acceptable and the average of the two values was taken as the official value. Otherwise, a further concentrated dye mother solution in DMSO was prepared, the whole procedure was repeated and the $\log \epsilon$ data were compared. The procedure continued until, comparing the values, a difference of 0.02 (on averaged $\log \epsilon$) or less, was attained.

2.2 Fluorescence Emission spectra and Fluorescence Quantum Yield

Fluorescence measurements were recorded using a Fluorolog 2 from Jobyn Ivon. The excitation wavelength was set at 600 nm. The range for fluorescence emission recording was from 610 to 850 nm. Excitation and emission slits (3 nm) were arranged in order that all fluorescence spectra could be recorded under the same conditions.

Few mg of dye was put in a test tube and few ml of proper solvent were added. The test tubes were sonicated from 30 sec to 1 min, and left to rest for about 30 minutes to accomplish complete solubilisation. The sample was used to prepare much diluted solutions, and their absorbance at λ_{\max} was determined in order to ensure that the absorbance is maintained lower of 0.1 units of absorbance. For every solution fluorescence emission spectrum was detected and λ_{em} was obtained. Two standards, Rhodamine 101 dissolved in EtOH/0.01 HCl and Cresyl Violet in MeOH, were measured under the same conditions of squaraine samples.

Operative conditions (Rhodamine 101 quantum yield = 1 and Cresyl Violet = 0.54)⁴:

- Rhodamine 101: $\lambda_{\text{ex}} = 535$, emission range: 545-800 nm, excitation and emission slits: 3 nm.

- Cresyl Violet: $\lambda_{\text{ex}} = 520$, emission range: 530-800 nm, excitation and emission slits: 3 nm.

The quantum yield⁵ is determined by:

$$\phi_x = \phi_{ST} \frac{A_x}{A_{ST}} \frac{I_{ST}}{I_x} \left(\frac{\eta_x^2}{\eta_{ST}^2} \right) \quad (\text{eq. 1})$$

where Φ_x is the measured quantum yield for the unknown sample, Φ_{ST} in the quantum yield of the standard reference (Rhodamine 101 or Cresyl violet) to which the measurement are referred, A_x and A_{ST} are the integrated areas under the fluorescence emission curve of the unknown sample and standard reference respectively, I_{ST} and I_x are the absorbance of the standard reference and unknown sample respectively, η_x and η_{ST} are the refractive indexes for the solvents in which the unknown sample and standard reference are dissolved respectively. The reported quantum yield is the average of the values obtained vs Rhodamine 101 and Cresyl Violet respectively.

2.3 Fluorescence lifetimes

Fluorescence lifetimes were obtained on a Fluorolog2 spectrofluorimeter, equipped with proper NanoLED source (emitting at 635nm) and using a photon counting detector (TBX04).

⁴ Magde, D; Brannon, J.H.; Cremers, T.L.; Olmsted, J. J. Phys. Chem. (1979), 83, 696-699.

⁵ Lakowicz JR. Principles of fluorescence spectroscopy. New York: Springer- Verlag; 2006.

The same solutions used for quantum yield determination were used. The data were fitted to a single exponential function giving the lifetime.

2.4 IR and Diffuse Reflectance Spectroscopy measurements

FT-IR spectra of dye powders were recorded in KBr pellets on a Shimadzu FT-IR Spectrometer (FTIR 8400). The resolution was set at 1 nm and the data were baseline subtracted and treated with triangle apodization function. Dyes adsorbed on TiO₂ electrodes were analysed using ATR (diamond, MKII Golden Gate) from Specac.

Diffuse reflectance spectrum was performed on a Cary 5000 UV-Vis-NIR Spectrophotometer. Electrodes for ATR were kindly provided by Solaronix within Innovasol project.

2.5 Electrochemistry

Voltammetric measurements employed a PC controlled AutoLab PSTAT10 electrochemical workstation and were carried out in an Ar-filled glove box, oxygen and water < 1 ppm. Cyclic Voltammetry and Differential Pulse Voltammetry techniques were used to estimate the redox potentials. CVs were obtained at a scan rate of 1 and 0.1 Vs⁻¹, DPVs were obtained at a Modulation Potential of 50 mV, a Step Potential of 10 mV, a Modulation Time of 50 ms and an Interval Time of 100 ms. Measurements were carried out using 0.1 M TBAPF₆ as supporting electrolyte in dimethylformamide (DMF); Glassy carbon, platinum plate and platinum wire were as working, counter and quasi-reference electrodes, respectively. At the end of each measurement, ferrocene was added as internal reference. We have considered the redox couple Fc⁺/Fc to be located at 0.628 V vs NHE accordingly to Hagberg and Mukherjee⁶.

2.6 Computational analysis of dye structure and electron distribution

Computational Analysis Geometry optimization has been carried out for SQ01-model and VG1-model (model systems in which the aliphatic chain has been substituted by a methyl moiety) at B3LYP/TZVP level in gas phase.

The geometrical structures of both dyes have been optimized *in vacuo* in “trans” and “cis” conformation with respect to the squarainic core: in the first case, the dihedral angles formed by the indolenine nitrogens and the squarainic core are 0 and 180 degrees, while in the second case they are both 0 degrees.

2.7 Cell assembly

A double layer film of interconnected mesoporous anatase TiO₂ particles was prepared by screen printing method upon 4 mm thick NSG10 TCO glass (Nippon Sheet Glass). The procedure for paste preparation and screen printing the electrodes is reported in⁷. The film was sensitized for 14 hours in darkness within a dye solution based of ethanol containing 100 μM of SQ01 or VG1C8 dye and with an increased concentration from 0 to 30 mM of cheno-deoxycholic acid as a co-adsorbant and de-aggregating agent. After being carefully washed by acetonitrile, the sensitized electrodes were sealed using a 25μm thick Surlyn gasket, melted by heating with a Pt-loaded TEC7 TCO counter electrode. The Pt was prepared by thermal degradation at 400°C during 15 minutes in air of a drop of 5 mM (H₂PtCl₆)_{EtOH} casted on the TCO surface. The internal space between the two electrodes was backfilled by electrolyte using a vacuum filling system. A hole was introduced in the counter electrode side by sand-blasting and was afterwards sealed with glass sheet. The electrolyte's composition is 0.6 M 1-butyl-3-methylimidazolium iodide, 0.05 M LiI, 0.04 M I₂, 0.275 M *tert*-

⁶ D. P. Hagberg, J.-H. Yum, H. Lee, F. De Angelis, T. Marinado, K. M. Karlsson, R. Humphry-Baker, L. Sun, A. Hagfeldt, M. Grätzel, Md. K. Nazeeruddin, *J. Am. Chem. Soc.*, 2008, **130**, 6259; L.M. Mukherjee, *J. Phys. Chem.* 1972, **76** (2), 243-245.

⁷ Ito S., Murakami T.N., Comte P., Liska P., Graetzel C., Nazeeruddin Md.K., Graetzel M., *Thin Solid Film* **2008**, 516(14), 4613-4619

butylpyridine and 0.05 M of guanidinium thiocyanate in a 85 / 15 % mixture by volume between acetonitrile and valeronitrile, respectively.

The printed photo-anode has a spot geometry with a surface area of 0.283 cm². Prior to measurements, the cell was masked with an aperture of 0.159 cm². Antireflection coating on the NSG10 glass was also used to prevent reflection losses.

2.8 Photovoltaic characterization

A 450 W xenon light source (Oriel, USA) was used to provide an incident irradiance of 100 mW/cm² at the surface of the solar cells. The spectral output of the lamp was filtered using Schott K113 Tempax sunlight filter (Präzisions Glas & Optik GmbH, Germany) that enables passing through light from 350 to 750 nm and hence to reduce light mismatch between real solar illumination and the simulated one to less than 2 %. Light intensities were regulated with wire mesh attenuators. The (J-V) measurements were performed using a Keithley model 2400 digital source meter (Keithley, USA) by applying independently external voltage to the cell and by measuring the photo-generated current out from the cell. Incident photon-to-current conversion measurements were realized using a 300 W xenon light source (ILC Technology, USA). A Gemini-180 double monochromator Jobin Yvon Ltd. (UK) was used to select and increment wavelength irradiation to the cell. The monochromatic incident light was passed through a chopper running at 1 Hz frequency and the on / off ratio was measured by an operational amplifier. This was superimposed on a white light bias corresponding to 10 mW/cm² intensity.

The cell capacitance was measured by charge extraction measurement. The electron lifetime was determined by transient photo-voltage decay measurements at open circuit. The white light bias, used to control the charge density within the mesoporous film, is generated by an array of LED's while a pulsed red light (0.05 s square pulse width) was triggered by a fast solid-state switch to ensure closed to equilibrium light perturbation. The subsequent voltage decay was recorded at open circuit condition on a mac-interfaced Keithley 2602 source meter. The resulting millisecond range decay was simulated by a single-exponential to extract the rate constant for electron recombination (s⁻¹) which was in turn inverted to electron lifetime (s) .

Dye loading

The dyes were adsorbed onto TiO₂ 5 micron thickness transparent electrodes for spectroscopy (courtesy of Solaronix). A dye solution based of ethanol containing 100 μM of SQ01 or VG1C8 dye and 20 mM of cheno-deoxycholic acid as a co-adsorbant and de-aggregating agent, was used. Absorption was checked by UV-Vis spectroscopy (Cary 300 Bio) and compared.

3. Optical characterization

3.1 UV-VIS

UV-VIS Spectra were collected for the squaraines using six different solvents: THF, dichloromethane (DCM), dimethylsulfoxide (DMSO), acetonitrile (ACN), ethanol (EtOH) and methanol (MeOH), in the concentration range $1 \cdot 10^{-6}$ - $5 \cdot 10^{-5}$ M. The spectra showed substantial negative solvatochromism: the λ_{\max} decreases when the solvent goes from low to high polarity. The solvatochromic behaviour is reported in Figure 2-SI and solvatochromic data are reported in Table 2-SI, while the $\log \epsilon$, FWHM (Full Width at Half Maximum) and the oscillator strength are reported in Table 3-SI. The length of the alkyl chain has no influence on the optical properties, whereas the presence of either one or two carboxylic functions conjugated to the chromogen induces a bathochromic shift of about 6-7 nm for each added group, resulting in a red shift for VG1 dyes respect to SQ01

In general, symmetrical structures exhibit higher molar extinction coefficient as well as higher oscillator strength in comparison to their asymmetrical counterparts. On the other hand, the presence or absence of carboxylic acid groups has no effect on this value.

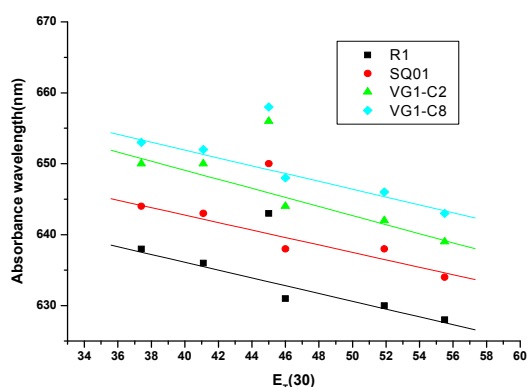


Figure 2-SI: negative solvatochromic behaviour for UV-Vis λ_{\max} vs $E_T(30)$, lines are from regression, excluding DMSO data.

Table 2-SI: Absorption maxima (λ_{\max}) for the squaraines in different solvents

Solvent	Dye			
	λ_{\max} [nm]			
	R1	SQ01	VG1-C2	VG1-C8
THF	638	644	650	653
DCM	636	643	650	652
DMSO	643	650	656	658
ACN	631	638	644	648
EtOH	630	638	642	646
MeOH	628	634	639	643

Table 3-SI: $\log \epsilon$, FWHM and oscillator strengths for the squaraines in different solvents

Solvent	R1			SQ01			VG1-C2			VG1-C8		
	$\log \epsilon$	FWHM	O. Str.									
		(nm)			(nm)			(nm)			(nm)	
THF	5.49	25	0.76	5.39	27	0.63	5.48	25	0.73	5.55	25	0.85
DCM	5.53	25	0.87	5.38	26	0.63	5.60	24	0.97	5.58	25	0.93
DMSO	5.42	27	0.70	5.21	28	0.41	5.45	26	0.73	5.45	29	0.80
ACN	5.45	26	0.77	5.30	29	0.58	5.44	24	0.72	5.55	26	0.94
EtOH	5.40	24	0.65	5.36	26	0.58	5.43	25	0.69	5.47	25	0.76
MeOH	5.50	25	0.82	5.39	27	0.67	5.47	24	0.74	5.49	25	0.78

The negative solvatochromism accounts for a higher polarity of the ground state with respect to the excited state. This is a standard situation for cyanine or cyanine-like chromogens⁸. Apolar solvents destabilize HOMO and stabilize LUMO thus obtaining a reduced band gap and longer absorption wavelength; the opposite occurs with polar solvents. When we tried to search for a linear dependence of the λ_{\max} vs $E_T(30)$ ⁹ for the different solvents, we found a good linearity (Figure 2-SI) except for DMSO.

A careful analysis of the λ_{\max} shift reveals that the addition of one carboxyl group (R1 vs SQ01), making the squaraine asymmetric, causes a shift of about 6 nm and that a second carboxyl causes a further red shift of 6 nm. This can be the result of the expansion of the conjugation above all the molecular skeleton due to the resonance ability of the carboxyl group.

A small red shift was observed within the VG1 series. With respect to VG1-C2, the λ_{\max} was slightly red shifted by the introduction of longer alkyl chains. At the first sight, this modification does not affect the conjugation and should not modify the chromogen. The effect was systematic, and for all chain lengths higher than ethyl (VG1-C2) the λ_{\max} is shifted by 2-4 nm, depending on the solvent. The reason of this effect is not clear at the moment.

Further important data were obtained from the UV spectra: the molar absorption, FWHM (Full Width at Half Maximum) and the oscillator strength f that are reported in Table 2-SI.

As a general trend, the molar absorption is not heavily affected for squaraines having symmetric structure, and remains unchanged in presence or absence of the carboxyl substituents (see: R1, without carboxyl groups, and the VG1 family, bearing carboxyls and variable hydrophobic chain length). Asymmetric (SQ01) structures, conversely, show a lower molar absorption. Taken as alone, those data could give the impression that asymmetrical squaraines would perform poorer from the absorption point of view. This is not the case, because further analysis of the table shows that the FWHM values remain in the same range for R1, SQ01 and VG1 series. The real strength in absorbing the light can be obtained by the oscillator strength. This was calculated according to the formula:¹⁰

$$f = 4.32 \cdot 10^{-9} \cdot \epsilon_{\max} \cdot FWHM [cm^{-1}] \quad (\text{eq. 2})$$

The oscillator strength, while varying for different solvents, is really reduced for SQ01. This accounts for a better ability of symmetric molecules to collect light than the asymmetric ones. Limiting the discussion to the absorption of light, this study seems to indicate that SQ01 should have lower performances than symmetric squaraines.

A study of the aggregation ability of those dyes was performed in EtOH, since this is the solvent used for dye absorption. The correlation with concentration was linear with excellent $r^2 = 0.995-0.999$ for SQ01 and VG1-C8. The aggregation was thus excluded, in the concentration range examined.

⁸ Gude C.; Rettig, W. *J. Phys. Chem. A* (2000),104, 8050-8057

⁹ C. Reichardt, *Chem. Rev.* **1994**, *94*, 2319 - 2358

¹⁰ Solvatochromism Suppan, P. and Ghoneim, G. eds Royal Society of Chemistry, Cambridge, 1997

3.2 Fluorescence Measurements

Fluorescence emission was studied in the same solvents used for the UV spectra. The dyes were studied from both the steady-state and time resolved emission point of view, to account for their properties. Fluorescence lifetimes and quantum yields increase at once by the presence of symmetry, the addition of COOH groups and the lengthening in the alkyl chains (Table 6-SI and Fig. 4-SI and 5-SI).

3.2.1 Emission spectroscopy

Spectra acquired in the different solvents gave the solvatochromic results reported in Figure 3-SI and the data are shown in Table 4-SI and 5-SI. The emission maximum, the Stoke's shift and the E_{0-0} transition were determined.

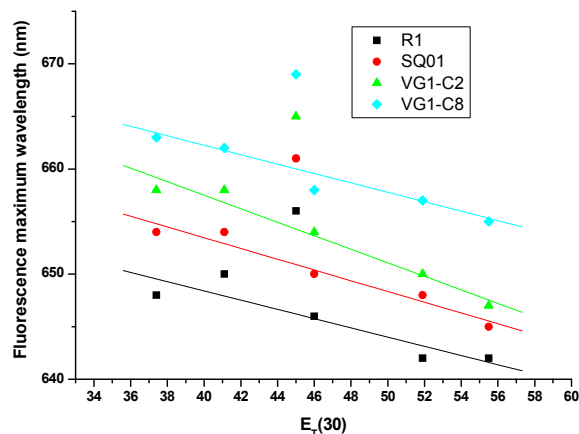


Figure 3-SI: Emission properties of squaraines), lines are from regression, excluding DMSO data.

Table 4-SI: Emission maxima (λ_{Max}) for the squaraines in different solvents

Solvent	Dye			
	R1	SQ01	VG1-C2	VG1-C8
THF	648	654	658	663
DCM	650	654	658	662
DMSO	656	661	665	669
ACN	646	650	654	658
EtOH	642	648	650	657
MeOH	642	645	647	655

Table 5-SI: Stoke's shifts and ΔE_{0-0} transitions for the squaraines in different solvents

Solvent	R1		SQ01		VG1-C2		VG1-C8	
	Stokes shift [nm]	ΔE_{0-0} [eV]						
THF	10	1.93	10	1.91	8	1.90	9	1.89
DCM	13	1.93	11	1.91	8	1.90	10	1.89
DMSO	12	1.91	11	1.89	9	1.88	13	1.86
ACN	15	1.95	11	1.93	10	1.91	12	1.90
EtOH	12	1.95	9	1.93	8	1.92	11	1.91
MeOH	13	1.96	10	1.94	8	1.93	11	1.91

The first study was devoted to analyze the solvatochromic behaviour of the squaraines. The negative solvatochromic behavior, already shown for the UV spectra, was evident also in the emission spectra. DMSO behaves anomalously also in this case. From the intersection of the absorption and emission spectra the zeroth-zeroth transition ΔE_{0-0} was evaluated. ΔE_{0-0} correlates with solvent polarity in accordance with the solvent polarity dependence for λ_{\max} . The transition gap increase (while λ_{\max} decreases) with solvent polarity. This confirms the more polar nature for the HOMO than for the LUMO. In agreement with the UV-VIS results, the insertion of a carboxyl increases the red shift of λ_{em} of about 3-6 nm (SQ01), a second carboxyl causes a further red shift of about 2-4 nm (VG1-C2). The effect of the elongation of hydrophobic chain within the compound belonging to the VG1 family is responsible for 4-8 nm red shift. As explained before for UV-VIS spectroscopy, the origin of this effect is presently unknown, and only a hypothesis can be made, as show above.

An analysis of the Stokes shifts shows that for the symmetrical squaraine R1 the Stokes shift is in the range of 8-12 nm. While it seems that the introduction of one carboxyl (from R1 to SQ01) does not have any particular effect on the E_{0-0} , the introduction of two carbonyls (VG1-C2) slightly reduces the E_{0-0} value and this is in agreement with a larger extension of the conjugation which is also reflected on the λ_{\max} red shift for those compounds. The reduction of E_{0-0} due to insertion of long alkyl chains is very small. Nonetheless this correctly follows the small red shifts occurring with the lengthening of the hydrophobic alkyl chain shown both by absorption and emission spectroscopy.

3.2.2 Fluorescence quantum yield and lifetime

The quantum yield determination gave the results shown in Table 6-SI, along with the results coming from time resolved studies.

Table 6-SI: Lifetime, quantum yield, Fluorescence constant and non-radiative constant for the squaraines

Solvent	R1				SQ01			
	τ	ϕ_{fl}	k_{fl}	k_{nr}	τ	ϕ_{fl}	k_{fl}	k_{nr}
	[ns]		$/10^7$ s^{-1}	$/10^7$ s^{-1}	[ns]		$/10^7$ s^{-1}	$/10^7$ s^{-1}
THF	0.979	0.300	30.64	71.50	0.975	0.506	51.90	50.67
DCM	0.743	0.260	34.99	99.60	0.640	0.359	56.09	100.16
DMSO	0.660	0.198	30.00	121.52	0.813	0.234	28.78	94.22
ACN	0.210	0.065	31.19	445.00	0.274	0.036	13.18	351.79
EtOH	0.506	0.137	27.08	170.55	0.649	0.267	41.14	112.94
MeOH	0.186	0.076	40.97	496.67	0.277	0.150	54.15	306.86

Solvent	VG1-C2				VG1-C8			
	τ	ϕ_{fl}	k_{fl}	k_{nr}	τ	ϕ_{fl}	k_{fl}	k_{nr}
	[ns]	Rh 101	$/10^7$ s^{-1}	$/10^7$ s^{-1}	[ns]		$/10^7$ s^{-1}	$/10^7$ s^{-1}
THF	1.133	0.695	61.34	26.92	1.518	0.541	35.64	30.24
DCM	1.265	0.562	44.43	34.62	1.359	0.457	33.63	39.96
DMSO	0.992	0.225	22.68	78.13	1.129	0.265	23.47	65.10
ACN	0.337	0.178	52.82	243.92	0.581	0.178	30.64	141.48
EtOH	0.832	0.275	33.05	87.14	1.086	0.350	32.23	59.85
MeOH	0.463	0.115	24.84	191.14	0.680	0.296	43.53	103.53

In order to examine the huge quantity of data it is better to refer to both Table 6-SI and the plots reported in Figure 4-SI. In general, the quantum yield increases due to insertion of carboxyls and long chains, as a consequence of the reduced mobility that the added moieties cause to the indolenine groups. Every modification that reduces the rotational ability of indolenine groups can help to increase quantum yield, lifetimes and thus, in principle, can be important to obtain better results in solar cells. When this rotation is inhibited, the quantum yield increases. The best plots were obtained reporting the quantum yield vs. Δf , this latter known as the Lippert parameter.¹¹ This is represented by equation 3:

$$\Delta f = (\epsilon - 1) / (2\epsilon + 1) - (n^2 - 1) / (2n^2 + 1) \quad (\text{eq. 3})$$

which contains both dielectric constant and refractive index, thus taking into account the aspects related to dipolar and dispersive forces into a solvent polarity scale. Values for the different solvents are: THF (0.210), DCM (0.218), DMSO (0.264), EtOH (0.289), ACN (0.306), MeOH (0.309).

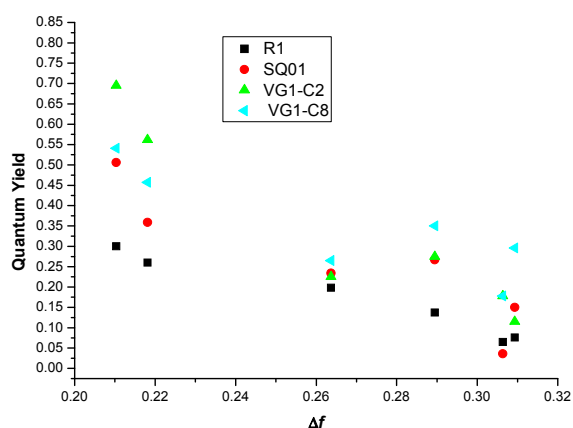


Figure 4-SI: Quantum yields of squaraines vs. Δf (Lippert parameter)

Lifetime measurements were performed in the above tested solvents. Fluorescence decay was fitted to a mono-exponential function and only in a few cases a double exponential function was used and however, the second lifetimes was giving little or no information since it accounted for 1-2% of the fluorescence decay, as a maximum. The analysis of the data contained in Table 6-SI shows that, in general, the increase of solvent polarity causes a reduction in the observed lifetime. The insertion of the first carboxyl group (from R1 to SQ01, also with an additional octyl chain) did not show any substantial increase in lifetime while the second carboxyl (from R1 to VG1-C2) caused the lifetime to increase. Also the further introduction of longer alkyl chains increased considerably the lifetime. VG1-C8 lifetime was nearly doubled with respect to the simple reference structure R1.

As a final confirmation, if we take into account of some relationships between quantum yield and lifetimes:

$$\phi_f = \frac{k_f}{k_f + k_{nr}} \quad (\text{eq. 4});$$

$$\tau = \frac{1}{k_f + k_{nr}} \quad (\text{eq. 5});$$

$$k_f = \frac{\phi_f}{\tau_f} \quad (\text{eq. 6})$$

$$k_{nr}^{tot} = k_f(\phi_f^{-1} - 1) \quad (\text{eq. 7})$$

we could obtain the constant that account for all the non-radiative processes that participate to the decrease of fluorescence. The k_{nr} vs Δf plot is reported in Figure 5-SI.

¹¹ Gude C.; Rettig, W. *J. Phys. Chem. A* (2000),104, 8050-8057

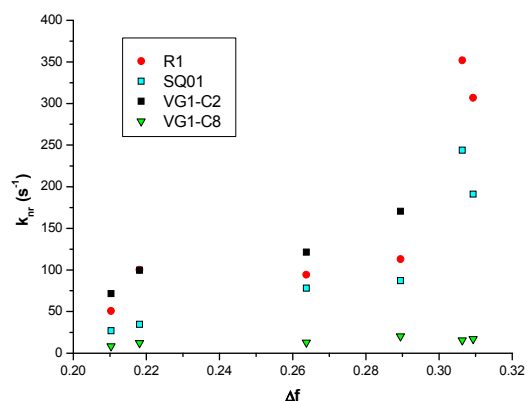


Figure 5-SI: Non-radiative constant vs Δf

It is easy to see that the non-radiative process that suppresses fluorescence is more efficient in polar solvents. However, the successive addition of longer alkyl chains onto the indolenines shows that those processes are reduced, in agreement with the previously demonstrated increase of both lifetimes and quantum yield.

In order to explain and rationalise our results, we can refer to a TICT (Twisted Intramolecular Charge Transfer state) mechanism, which was first proposed for cyanine and was found to work also for squaraines to account for the very short lifetimes and low quantum yield.¹² This TICT mechanism¹³ (see Figure 6-SI) also accounts for the substantial higher reduction of squaraine lifetimes obtained in polar solvents with respect to less polar ones.

It is easier to explain why both lifetimes and quantum yields are increasing by the successive addition of carboxyl and long alkyl chain onto the indolenines. The addition of only one carboxyl and one alkyl chain into a single indolenine (from R1 to SQ01) does not show nearly any effect because one of the two indolenines remains unchanged and this will be the favoured moiety that will rotate, thus making the fluorescence to be efficiently reduced. The simple addition of two carboxyl groups, one for every indolenine, will reduce the rotational ability of both moieties, thus rising lifetimes and quantum yields. The introduction of one alkyl chain per indolenine moiety

¹² Tatikolov, A.S.; Costa, S.N.B. *J. Photochem. Photobiol.* (2001), 140, 147-156; b) Gude C.; Rettig, W. *J. Phys. Chem. A* (2000), 104, 8050-8057; c) Rettig, W. In *Electron Transfer I*; Mattay, J., Ed.; Topics in Current Chemistry, Vol. 169; Springer-Verlag: Berlin, 1994

¹³ In the general Jabloski diagram, ground and excited state are represented by energy levels. Those levels correspond to a minimum in an energy curve. The excited state is higher in energy than ground state and its curve is in general a bit shifted to the right along the x coordinate, accounting for a change in molecular geometry. From this situation, after the adsorption and the relaxation to the lower vibrational level of the excited state, the fluorescence emission occurs, taking the molecule back to its ground state. When a molecule possesses a long conjugate system it is possible that in the excited state one of the double bonds of the conjugated system can be broken thus permitting to different moieties of the molecule to rotate one with respect to the other. In this case, in the excited state a charge separation occurs, giving a dipolar nature to the molecule since its two twisted moieties have opposite charges. This is usually occurring for a 90° twisted excited state, while its corresponding 90° twisted ground state will be on a maximum since it is impossible to freely rotate two moieties around a double bond in the ground state. In fig 8-SI we are observing the ground and excited state energy diagram along a rotation coordinate that express the rotation angle of the two indolenine moieties of the squaraine. Starting from the planar (0°) conformation, the excited state can evolve towards the twisted conformation (90°) and the involved energetic barrier is quite easy to be overcome even at room temperature. In those conditions the planar conformation of the excited state can be substantially depopulated by conversion to the twisted 90° conformation. Since this latter conformation is very close to the maximum of the ground state, a non-radiative deactivation of the excited state to the ground state can occur. Due to this pathway, the excited planar state is greatly depopulated and cannot show fluorescence anymore. In fact, only the few molecules in the planar conformation can give fluorescence. This accounts for both short lifetimes and low quantum yield normally observed for squaraines. In particular, since the twisted 90° conformation of the excited states has a polar nature, this will be greatly stabilized by polar solvents.

(from R1 to VG1-C2) will give further reduction of rotational mobility and as a result, the fluorescence lifetimes and quantum yield will increase.

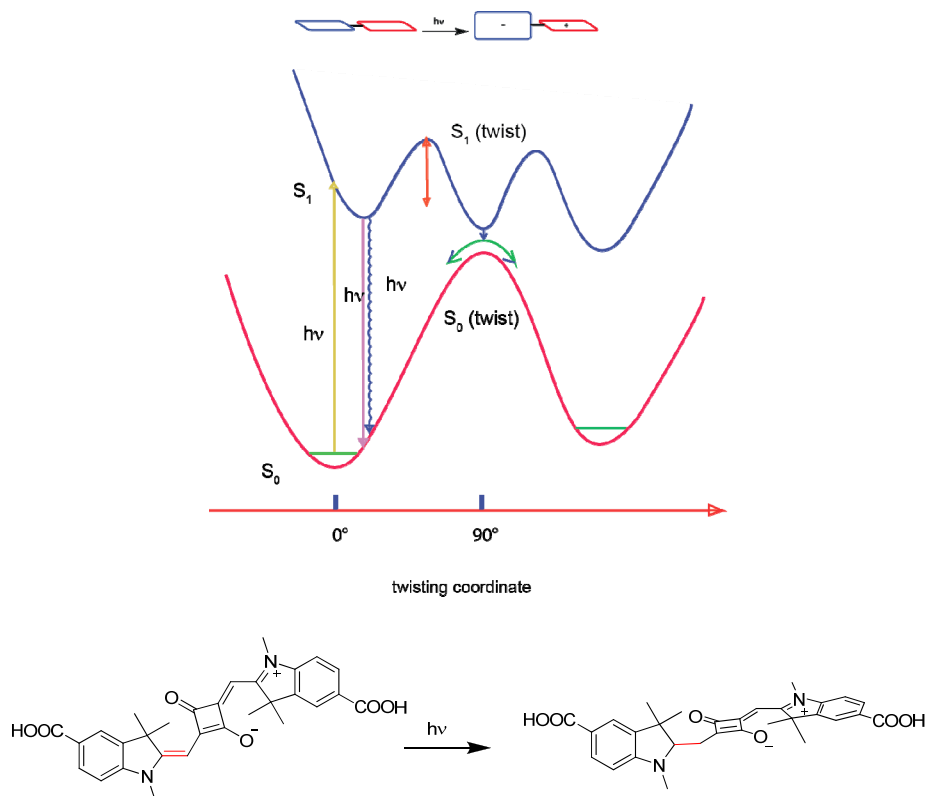


Figure 6-SI: Energy Diagram of the ground and excited state for a squaraine dye involved in the formation of a TICT state

4 Dyes adsorption on TiO₂

Dyeing of TiO₂ supported on TCO glass

The dyes were adsorbed onto TiO₂ supported on TCO glass.

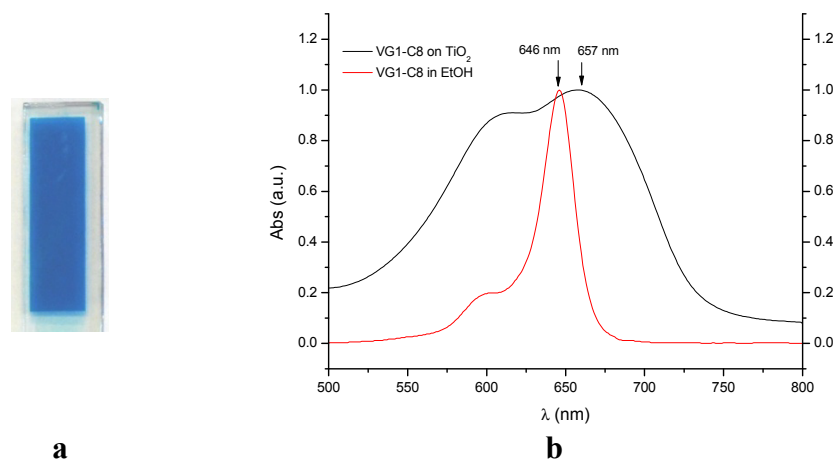


Figure 7-SI: a) VG1-C8 adsorbed on TiO₂ electrode and b) reflectance spectrum of VG1-C8 adsorbed on TiO₂ compared to VG1-C8 in ethanol solution.

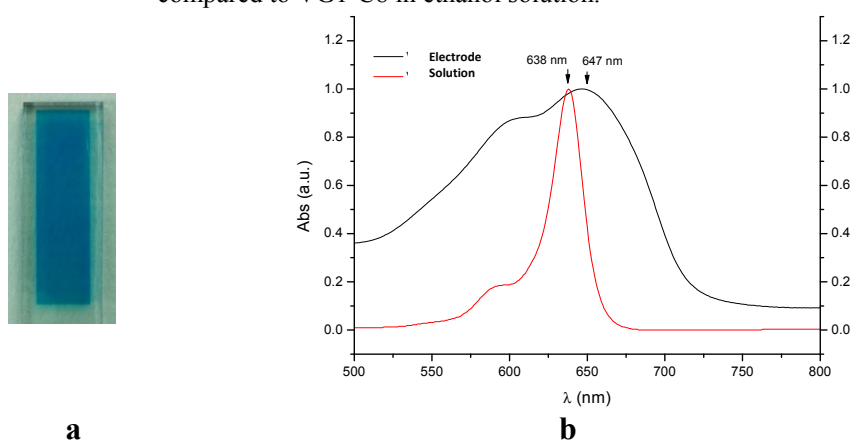


Figure 8-SI: a) SQ01 adsorbed on TiO₂ electrode and b) reflectance spectrum of SQ01 adsorbed on TiO₂ compared to SQ01 in ethanol solution.

The adsorption is uniform and relatively stable.

5 FT-IR and ATR analysis

After dye adsorption, the dried electrodes were used to measure ATR spectrum. The reference spectrum of pure dye was measured using FT-IR on dye powder diluted in KBr pellets.

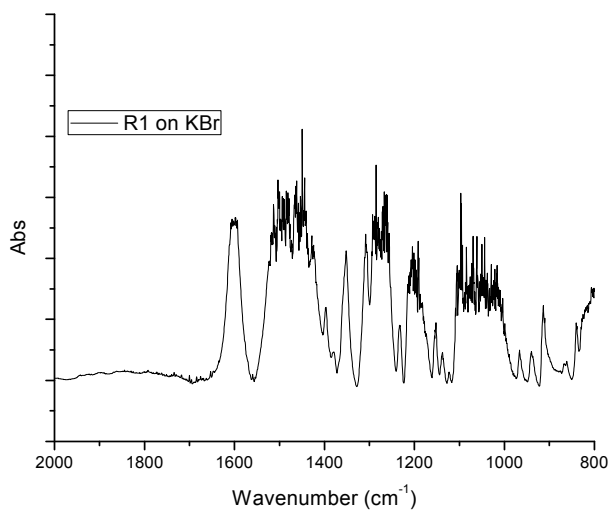


Figure 9-SI: FT-IR spectrum of R1 on KBr.

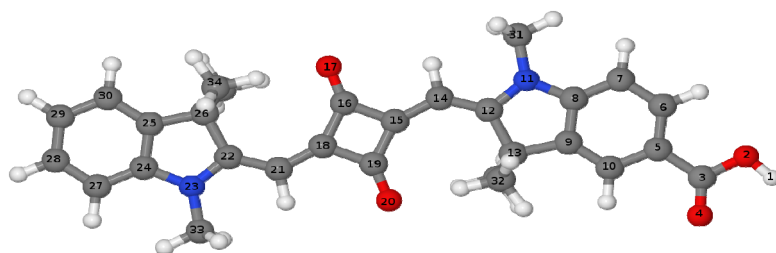
In Fig. 9-SI the spectrum of the reference squaraine R1 (without COOH groups) is reported in order to identify the characteristic peaks of squaraine structure.

6 Computational analysis of dye structure and electron distribution

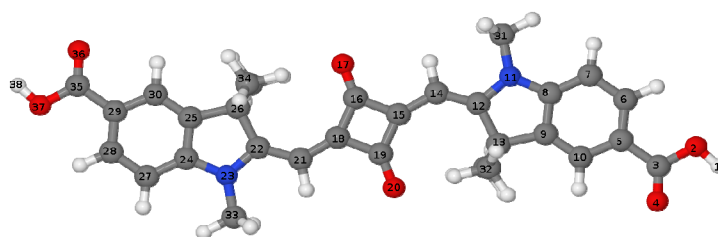
All relaxed geometries show a planar structure. VG1-model has a C_{2s} symmetry in both *cis* and *trans* conformations. In Table 7-SI main geometrical parameters are collected. The computed electric dipole moments for the ground states are 3.49 debye and 3.32 debye for *trans* and *cis* conformations of SQ01-model, respectively, and 0.05 debye and 4.03 debye for *trans* and *cis* conformations of VG1-model. It is important to notice how the *trans-cis* rotation enhance the polarity of VG1-model to values higher than SQ01-model.

In Table 8-SI the vertical excitation energies (VEE) and the wavelengths corresponding to the transitions that dominate the visible absorption spectra are collected.

Table 7-SI: Main geometrical parameters for *cis*- and *trans*- isomers of SQ01-model and VG1-model. Distances are in angstrom. Schematic drawings of model molecules with label numbering are shown.



SQ01-model



VG1-model

	SQ01-model <i>trans</i>	SQ01-model <i>cis</i>	VG1-model <i>trans</i>	VG1-model <i>cis</i>
O2-H1	0.97	0.97	0.97	0.97
O2-C3	1.36	1.36	1.36	1.36
C3-O4	1.21	1.21	1.21	1.21
C3-C5	1.48	1.48	1.47	1.47
C5-C6	1.40	1.40	1.40	1.40
C6-C7	1.39	1.39	1.39	1.39
C7-C8	1.39	1.39	1.38	1.38
C8-C9	1.40	1.40	1.40	1.40
C9-C10	1.38	1.38	1.38	1.38
C8-N11	1.41	1.41	1.41	1.41
N11-C12	1.49	1.49	1.49	1.49
C12-C13	1.38	1.38	1.38	1.38
C13-C9	1.53	1.53	1.54	1.54

C12-C14	1.52	1.52	1.52	1.52
C14-C15	1.38	1.38	1.38	1.38
C15-C16	1.40	1.40	1.40	1.40
C16-O17	1.47	1.47	1.47	1.47
C16-C18	1.23	1.23	1.23	1.23
C18-C19	1.48	1.48	1.48	1.48
C19-O20	1.47	1.47	1.47	1.47
C19-C15	1.23	1.23	1.23	1.23
C18-C21	1.47	1.47	1.46	1.46
C21-C22	1.39	1.39	1.39	1.39
C22-N23	1.38	1.38	1.38	1.38
N23-C24	1.37	1.37	1.37	1.37
C24-C25	1.41	1.41	1.42	1.42
C25-C26	1.39	1.39	1.38	1.38
C26-C22	1.52	1.52	1.52	1.52
C24-C27	1.39	1.39	1.39	1.39
C27-C28	1.39	1.39	1.39	1.39
C28-C29	1.39	1.39	1.39	1.39
C29-C30	1.40	1.40	1.40	1.40
C30-C25	1.38	1.38	1.38	1.38
N11-C31	1.45	1.45	1.45	1.45
C13-C32	1.55	1.55	1.55	1.55
N23-C33	1.45	1.45	1.45	1.45
C26-C34	1.55	1.55	1.55	1.55
C29-C35			1.48	1.48
C35-O36			1.21	1.21
C35-O37			1.36	1.36
O37-H38			0.97	0.97
O2-C3-O4	121.9	121.9	121.9	121.9
C3-C5-C6	122.1	122.1	122.1	122.1
C6-C7-C8	117.8	117.8	117.7	117.7
C8-N11-C12	112.2	112.2	112.2	112.2
C8-C9-C10	119.9	119.9	119.9	119.9
C12-C13-C9	101.0	101.0	101.0	101.0
C12-C14-C15	132.4	132.4	132.4	132.4
C14-C15-C16	125.6	125.6	125.6	125.6
C15-C16-O17	133.2	133.2	133.2	133.2

C15-C16-C18	90.0	90.0	90.0	90.0
C16-C18-C19	89.7	89.7	89.7	89.7
C18-C19-O20	132.6	132.6	132.5	132.5
C16-C18-C21	144.8	144.8	144.8	144.8
C18-C21-C22	132.2	132.2	132.2	132.2
C22-C26-C25	101.4	101.4	101.4	101.4
C22-N23-C24	111.7	111.7	111.7	111.7
C24-C25-C30	119.8	119.8	119.8	119.8
C27-C28-C29	121.1	121.1	121.2	121.2
C24-N23-C33	124.0	124.0	124.0	124.0
C28-C29-C35			122.1	122.1
C29-C35-O36			125.0	125.0
O36-C35-O37			121.7	121.7
O2-C3-O4-C5	180.0	180.0	180.0	180.0
O2-C3-C5-C6	0.0	0.0	0.0	0.0
C5-C6-C7-C8	0.0	0.0	0.0	0.0
C7-C8-C9-C10	0.0	0.0	0.1	0.1
C7-C8-N11-C12	180.0	180.0	180.0	180.0
C7-C8-N11-C31	0.0	0.0	0.0	0.0
N11-C12-C13-C9	0.0	0.0	0.0	0.0
N11-C12-C14-C15	180.0	180.0	180.0	180.0
C12-C14-C15-C16	180.0	180.0	180.0	180.0
C14-C15-C16-O17	0.0	0.0	0.0	0.0
C14-C15-C16-C18	180.0	180.0	180.0	180.0
C16-C18-C19-O20	180.0	180.0	180.0	180.0
C16-C18-C21-C22	0.0	179.9	0.0	179.9
C18-C21-C22-C26	0.0	0.0	0.0	0.0
C21-C22-C26-C25	180.0	180.0	180.0	180.0
C22-C26-C25-C24	0.0	0.0	0.0	0.0
C26-C25-C24-N23	0.0	0.0	0.0	0.0
C25-C24-N23-C33	180.0	180.0	180.0	180.0
C24-C25-C30-C29	0.0	0.0	0.0	0.0
C27-C28-C29-C35			180.0	180.0
C28-C29-C35-O36			179.8	179.8
C29-C35-O36-O37			180.0	180.0

Table 8-SI: Main transitions for SQ01 and VG1 models in gas phase.

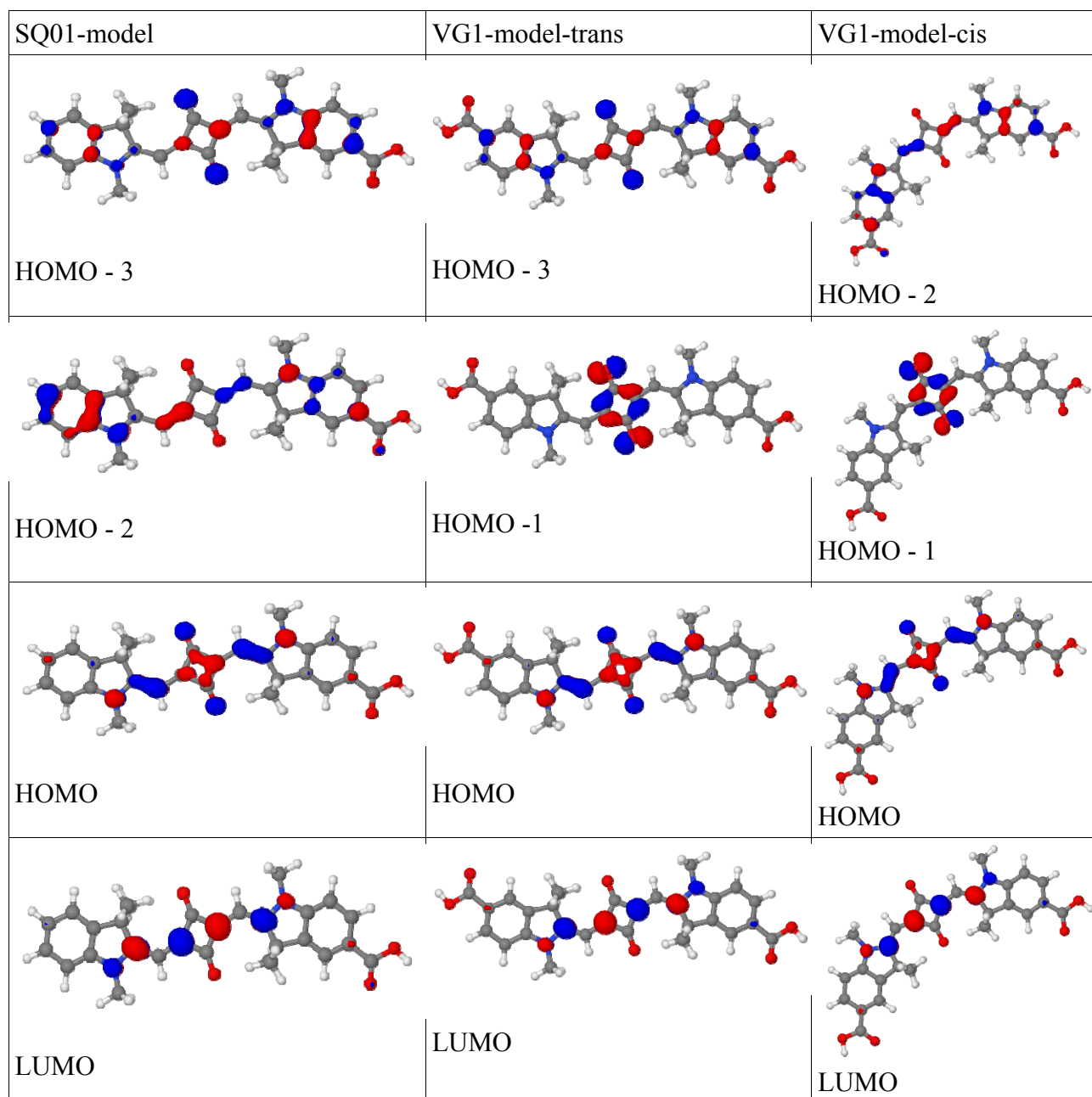
	VEE (eV)	Lambda (nm)	Osc. Str.	transitions		%
SQ01-model trans	2.26	547	1.47	124 (HOMO)	125 (LUMO)	98
	3.24	382	$1.03 \cdot 10^{-2}$	124	126	81
				122	125	16
	3.48	356	$1.35 \cdot 10^{-1}$	121	125	64
				122	125	30
SQ01-model cis	2.25	550	1.38	124 (HOMO)	125 (LUMO)	98
	3.24	383	$2.47 \cdot 10^{-2}$	124	126	81
				122	125	16
	3.47	357	$1.39 \cdot 10^{-2}$	121	125	67
				122	125	27
VG1-model trans	2.22	559	1.54	135 (HOMO)	136 (LUMO)	97
	2.28	545	$1.94 \cdot 10^{-3}$	134	136	99
	3.41	363	$8.14 \cdot 10^{-2}$	135	138	56
				132	136	44
VG1-model cis	2.21	562	1.37	135 (HOMO)	136 (LUMO)	97
	2.22	558	$4.41 \cdot 10^{-3}$	134	136	99
	3.18	390	$4.28 \cdot 10^{-2}$	135	137	82
				133	136	18

It has been shown¹⁴ that TD-DFT calculations usually overestimate the excitation energies of the π/π^* transition for highly delocalized organic dyes, but the errors are mostly systematic and can be corrected using appropriate linear scaling approaches. The remaining difference with respect to the experiment comes from the effects of the surrounding media and from the limitation of the exchange-correlation functional. In this case, the average difference between calculated and experimental results (considering experimental data collected in THF) is equal to 0.4 ± 0.04 eV. However, with these factors constant and due to the computational method, the comparison between optical properties of different dyes is made possible by the reliability of the trends of the computed data.

The presence of the second carboxylic moiety induces a bathochromic shift of 0.04 eV (12 nm) for both the *trans* and *cis* couples. The oscillator strength is higher for *trans* VG1-model compared to the corresponding *trans* SQ01-model, while it is comparable for the *cis* conformations. On the other hand, the *trans-cis* rotation provides very small differences (0.01 eV, 1 nm) in the main electronic transitions for each dye model.

¹⁴ Champagne B, Guillaume M, Zutterman F. TDDFT investigation of the optical properties of cyanine dyes. Chemical Physics Letters 2006;425:105–9

For SQ01-model the effect of the different conformations on the minor contributions to the absorbance spectrum seem to be scarcely noticeable (1 nm) and the molecular orbitals involved are the same. On the contrary, VG1-model spectra show differences in the energy levels, oscillator strength and contributions of the minor transitions. In particular, the second root has transition energy 2.28 eV (545 nm) for trans VG1-model and 2.22 eV (558 nm) for cis VG1-model, while the third root has transition energy 3.41 eV (363 nm) for trans VG1-model and 3.18 eV (390 nm) for *cis* VG1-model. The oscillator strength for the trans conformation is almost double than the cis. The electron density of the frontier orbitals involved in the UV–Visible spectra is sketched in Figure 10-SI.



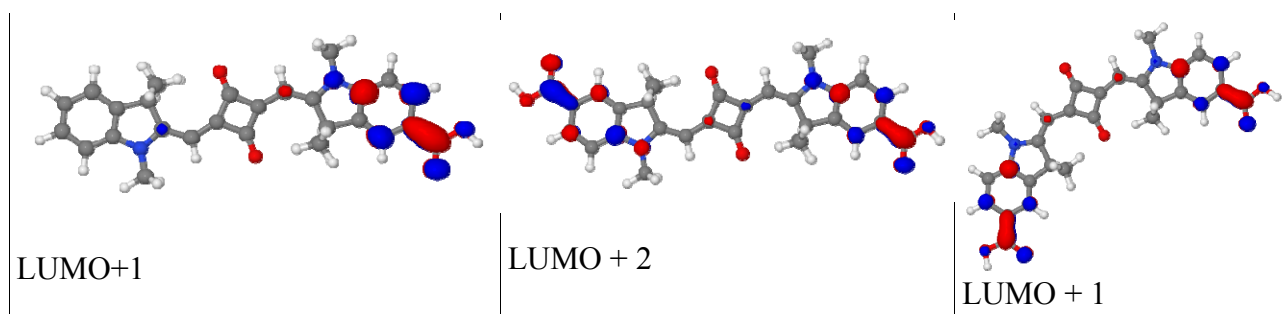


Figure 10-SI: Molecular orbitals involved in the main electronic transitions.

In all cases, the electron density is highly delocalized involving the squarainic core, the carbon chain, the indole rings and the carboxylic moieties, while the alkyl chains have negligible contributions to the molecular orbitals involved in the absorption spectra.

In all cases, the frontier orbitals are localized mainly on the squarainic ring and on a small portion of the indole rings (first carbon and nitrogen atom). All LUMOs are characterized by a very small electron density on carboxylic oxygens. Lower energy orbitals are highly delocalized, with the exception of HOMO-1 orbital in VG1-model, in which the electron density is completely localized on the squarainic core.

Molecular orbitals showing high electron density on the COOH moieties are high-energy orbitals, such as LUMO+1 (for SQ01-model and cis VG1-model) and LUMO+2 (trans VG1-model).

7 Electrochemical Properties—Cyclic Voltammetry

In analogy to its optical properties, the electrochemical properties of the symmetrical sensitizer VG1-C8 slightly differ from the electrochemical properties of the non symmetric SQ01. The cyclic voltammograms of both sensitizers show quasi-reversible peaks.

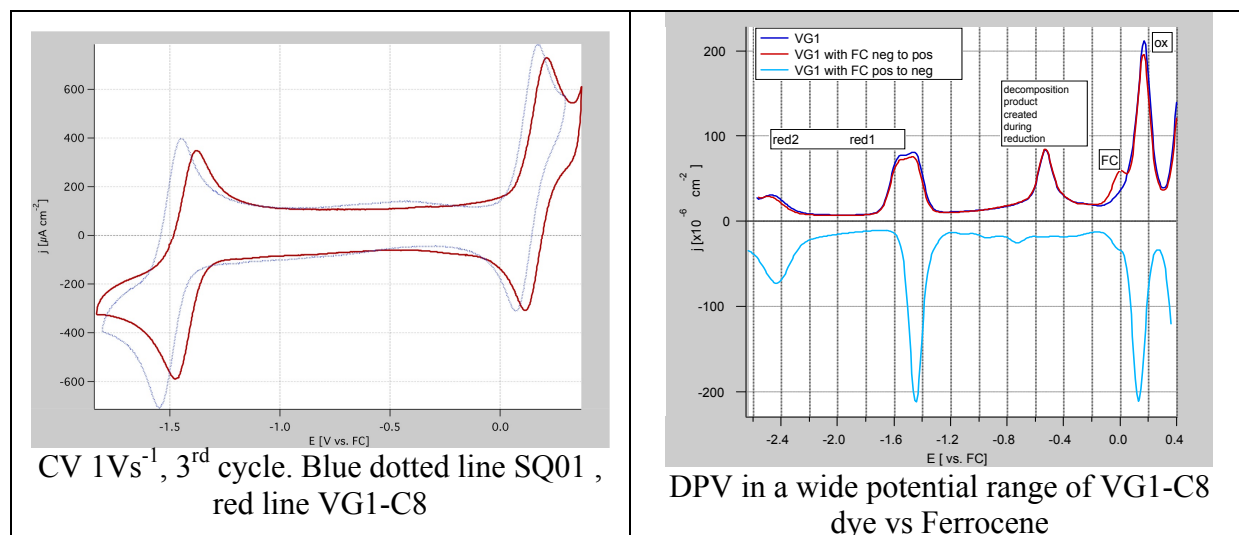


Figure 11-SI: Electrochemical properties of VG1-C8 compared to SQ01.

The measured redox potential is used as an estimation of E° . We assumed that the first oxidation potential (E_{ox}^0) and reduction potential (E_{red}^0) corresponds to the HOMO and, with a larger approximation, to LUMO levels of the dyes. Therefore, using the conversion factor of Fc+/Fc 0.63 V vs NHE, the HOMO and LUMO levels are located at 0.74 and -0.87 V versus NHE for **SQ01** and at 0.79 and -0.8 V versus NHE for **VG1-C8**, respectively. In the literature, the LUMO is also calculated by subtracting the value of the optical band gap E_g^{opt} from the value of the oxidation potential E_{ox}^0 . This method provides the LUMOs of the dyes located at even lower levels (**VG1-C8**: $E_{ox}^0 - E_g^{opt} = -1.02V$ vs. NHE, **SQ01**: $E_{ox}^0 - E_g^{opt} = -0.96V$ vs. NHE).

8 Photovoltaic characterization

Table 9-SI: Photovoltaic characteristics recorded for **SQ01** and **VG1-C8** dye as a function of the cheno-deoxycholic acid concentration in dye solution.

<i>[cheno]</i> mM		0	1	5	10	20	30
SQ01	<i>J_{sc}</i> (mA/cm ²)	7.1	7.2	7.8	7.7	8.5	8.0
	<i>V_{oc}</i> (mV)	608	599	624	654	641	653
	<i>ff</i>	0.75	0.74	0.77	0.78	0.78	0.78
	<i>η</i> (%)	3.3	3.3	3.7	3.9	4.2	4.1
VG1-C8	<i>J_{sc}</i> (mA/cm ²)	6.0	6.9	7.4	7.1	9.4	8.1
	<i>V_{oc}</i> (mV)	594	606	617	613	629	638
	<i>ff</i>	0.76	0.77	0.77	0.77	0.77	0.78
	<i>η</i> (%)	2.7	3.2	3.5	3.4	4.6	4.1

Figure 12-SI compares the evolution of the cell capacitance as a function of photo-voltage between the two dyes.

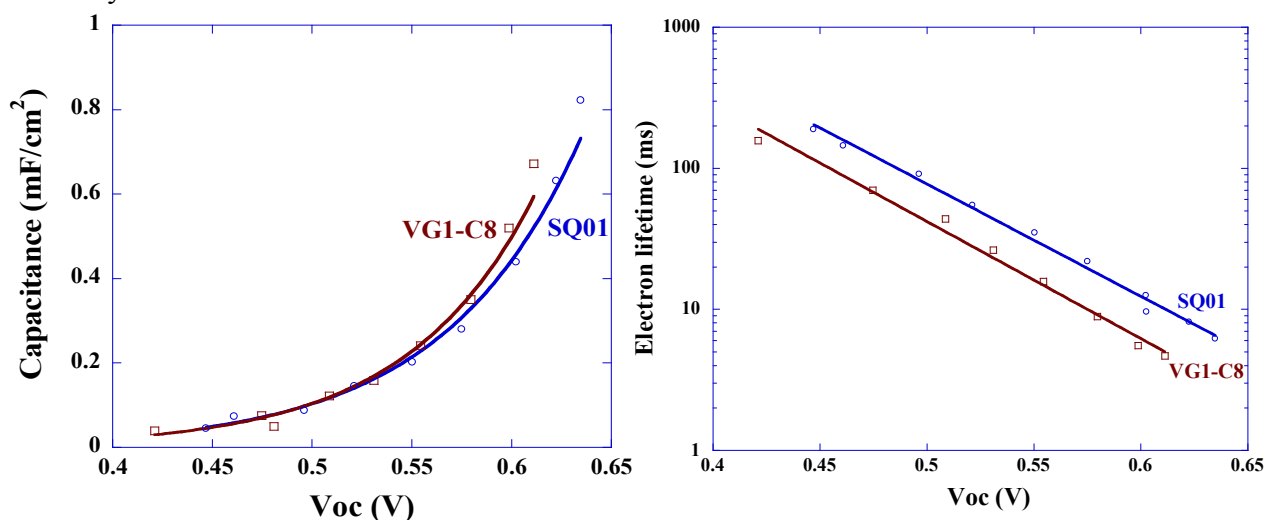


Figure 12-SI: Comparison of the cell capacitance (left) and electron lifetime (right) as a function of photo-voltage for **SQ01** and **VG1-C8** dye.

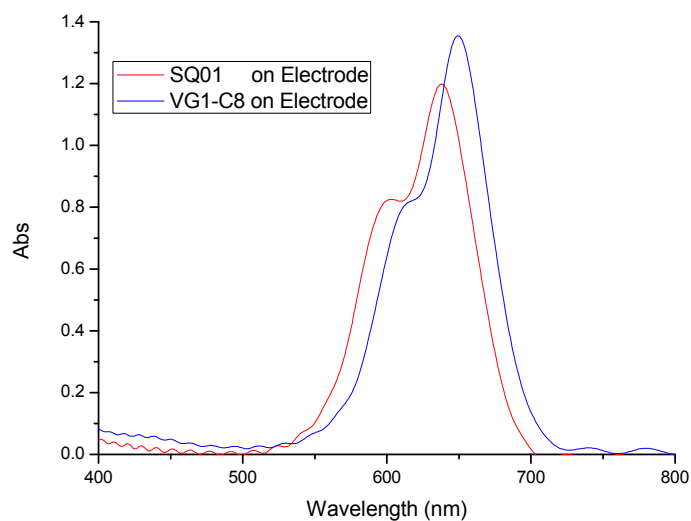


Figure 13-SI: Comparison of the absorption spectra on TiO_2 transparent electrodes of **SQ01** and **VG1-C8** dye after the same time of absorption from dye loading solution.

Dye loading was investigated by simple comparison between the absorption spectra of the two dyes on transparent electrodes (Solaronix) after different immersion times. Considering the lower (about 20% less) molar extinction coefficient of SQ01 respect to VG1-C8 the quantity of dye on the electrode is slightly higher for SQ01 (1.2 vs 1.35 unit of absorbance respectively for SQ01 and VG1-C8), but the absorption at higher wavelengths is higher for VG1-C8, probably due to a different conformation of the two dyes on the surface, while the two dyes have absolutely the same behavior at these wavelengths in solution. Figure 13-SI compares the absorption spectra on TiO₂ transparent electrodes of the two dyes after the same time of absorption from dye loading solution (100 μM of SQ01 or VG1C8 dye + 20 mM of cheno-deoxycholic acid).